

Research article

Iron electrolysis inhibits filamentous overgrowth in polymer-fed aerobic granular sludge system: Iron-electricity synergistic effect and mechanism



Mingyue Geng^a, Deyi Kong^a, Shanshan Gao^a, Fangshu Qu^{b,*}, Jiayu Tian^{a,**}

^a School of Civil and Transportation Engineering, Hebei University of Technology, Tianjin, 300401, China

^b School of Environment and Energy Engineering, Beijing University of Civil Engineering and Architecture, Beijing, 100044, China

ARTICLE INFO

Keywords:

Aerobic granular sludge
Filamentous overgrowth
Iron electrolysis
Electron transfer
Microbial community

ABSTRACT

Polymers comprise a significant fraction of organics in domestic wastewater, yet their slow hydrolysis seriously limits intracellular substrate storage, leading to excessive filamentous growth and destabilization of aerobic granular sludge (AGS). This study investigated the application of iron electrolysis to inhibit filamentous overgrowth in polymer-fed AGS reactor. Results showed that the AGS developed in the control reactors exhibited fluffy structure with excessive filament growth on the granule surface. On the contrary, iron electrolysis inhibited filamentous structure development, resulting in the granules exhibiting smooth edge, stable particle size (~1.8 mm), high biomass retention (9.0 ± 0.2 g/L) and superior settleability (SVI₅: 29–35 mL/g) throughout a 200-day operation. Further investigation revealed that iron electrolysis improved the activities of hydrolytic enzymes (α -amylase: 2905 U/gVSS; protease: 31.4 U/gVSS) and increased the synthesis of poly-hydroxybutyrate (20.6 ± 1.6 mg/gVSS). Moreover, electrochemical property analysis showed that the granules formed under iron electrolysis displayed high specific capacitance (4.1 ± 0.3 mF/g) and low charge transfer resistance (680Ω), displaying strong electron transfer capacity. Microbial assembly analysis demonstrated that iron electrolysis inhibited the growth of filamentous bacteria of *Herpetosiphon*, and increased the relative abundances of hydrolytic/fermentative bacteria (norank_o_Saccharimonadales: 7.5–13.1 %; *Lactococcus*: 2.1–4.8 %; *Tetrasphaera*: 4–4.8 %) and electroactive bacteria (*Clostridium_sensu stricto_13*: 6–6.7 %; *Trichococcus*: 5.9–7.1 %).

1. Introduction

Aerobic granular sludge (AGS) has been extensively studied over the past 30 years, emerging as a promising alternative to conventional activated sludge systems due to its advantages, including high biomass retention, excellent settling performance, great resistance to shock load (Han et al., 2022; Franca et al., 2018).

It is known that real domestic wastewater primarily consists of polymers, including carbohydrates, proteins and lipids (Toja et al., 2021; Kong et al., 2022). A large number of studies have proved that feeding with polymers drove filamentous overgrowth, destabilizing granule structure and significantly hindering the long-term operation of AGS technology during engineered application. For instance, de Kreuk et al. (de et al., 2010) used starch as a model polymeric substrate to culture granules and observed that the resulting granules exhibited a filamentous and fluffy morphology with poor sludge settleability. Likewise, Chen et al. (2024) reported that the introduction of starch led to

filamentous granules characterized by a notable abundance of the filamentous genus *Kouleothrix*. Geng et al. (2025) demonstrated that feeding AGS reactor with polymers stimulated the formation of filamentous structures and poorly settling flocs. The development of such fluffy or filamentous structures is undesirable, as it results in poor sludge settleability and biomass loss, ultimately leading to operation collapse of AGS reactor. According to metabolic selection theory, the filamentous overgrowth in polymer-fed AGS systems should be attributed to the weak storage of influent substrates as poly-hydroxybutyrate (PHB) anaerobically by functional microbes, such as polyphosphate/glycogen-accumulating organisms (PAO/GAO) (Winkler et al., 2011; Guzmán et al., 2023). Unlike simple substrates, polymers cannot be directly consumed by microbes, which need to be hydrolyzed/fermented into smaller molecular weight compounds before uptake by PAO/GAO. The slow hydrolysis limited PHB storage, which created a nutrient-rich environment (extracellularly) for microbes. This provides a great condition for the overgrowth of filamentous bacteria,

* Corresponding author.

** Corresponding author.

E-mail addresses: qufangshu@163.com (F. Qu), tjy800112@163.com (J. Tian).

and leads to the bulking of AGS (de et al., 2010; Geng et al., 2025).

To date, lots of methods have been reported to inhibit filamentous overgrowth, mainly including operational parameter optimization, chemical inhibitor dosage, quorum sensing regulation, etc. For example, Amancio Frutuoso et al. (Amancio et al., 2025) demonstrated that increasing selection pressure (such as shortening settling time, reducing sludge retention time) could wash out the filamentous bacteria with poor settleability but risk biomass loss. Liang et al. (2025) reported that heavy metal (such as iron salt) dosage exhibited toxic effects on filamentous bacteria and thus inhibited the overgrowth of filaments. Besides that, researchers successfully applied quorum sensing technology to disrupt the bacterial communication and regulate filamentous bacteria behaviors, inhibiting filamentous bulking phenomenon (Lu et al., 2023). However, current strategies predominantly targeted the physiological traits of filamentous bacteria (e.g., washing out the poor-settleability filamentous bacteria, exerting toxic effects on filamentous bacteria), limited studies focused on the driver of filamentous bulking in polymer-fed AGS systems: the weak conversion of influent polymers into intracellular storage polymers like PHB.

Iron electrolysis integrated iron and electricity, which has been demonstrated to be an effective strategy for enhancing the performance of AGS systems. Firstly, electric fields can regulate microbial metabolic behaviors and promote the granulation process through electrophoresis (Li et al., 2024). Secondly, iron ions released from the iron anode can be adsorbed and deposited within the granules, forming inorganic precipitates that strengthen granule structure and stability (Nanchariah and Kiran Kumar Reddy, 2018). For example, He et al. (2024) reported that applying an electric field stimulated extracellular polymeric substance (EPS) secretion by altering cell membrane permeability, thereby reducing the duration of granule formation in acetate-fed AGS system. Guo et al. (2021) found that iron electrolysis optimized nutrient (nitrogen and phosphorus) metabolism and intensified the structural strength of granules, which contributed to the stability of acetate-fed AGS system. However, most of the applied scenarios primarily utilized simple organic matter as substrates. The potential of using iron electrolysis to enhance influent polymer conversion into PHB and thereby inhibit filamentous bacteria overgrowth has not yet been explored.

This study was based on the hypothesis that iron electrolysis inhibited filamentous overgrowth in polymer-fed AGS system. First, the sludge properties were investigated during a 200-day operation period to assess the feasibility of applying iron electrolysis to inhibit the overgrowth of filamentous structures in polymer-fed AGS. Second, the polymer removal, hydrolytic enzyme activity and PHB storage were determined to analyze the effects of iron electrolysis on influent polymer conversion into PHB. Third, the electron transfer capacity and microbial assembly were investigated to explore the underlying mechanisms.

2. Materials and methods

2.1. Experiment setup and reactor operation

Four cylindrical sequencing batch reactors (SBRs, ϕ 10 cm \times 80 cm) with a working volume of 6.3 L were operated in this study. The four reactors were named as R_C (without iron and electricity), R_E (electricity alone), R_{Fe} (iron ions alone) and R_{IE} (both iron and electricity), respectively. R_{IE} was equipped with inert cathode and iron anode (ϕ 3 mm \times 100 mm). In R_E, an iridium-containing titanium rod was used as anode instead of iron rod. The electrodes were connected with a direct current (DC) power source applying voltage of 1.5 V. In R_{Fe}, no electrode was applied and Fe²⁺ was introduced into reactor. The dosage of Fe²⁺ was determined according to Faraday's law of electrolysis (~16.8 mg/L).

Four SBR reactors were operated continuously for 200 days with a cycle time of 240 min, comprising 120 min for feeding, 85–110 min for aeration, 5–30 min for settling and 5 min for discharging. Influent was pumped from the reactor bottom. The air flow rate was controlled at 2.5

L/min during aeration period. Solenoid valves were installed at a height of 40 cm to regulate effluent discharge, resulting in hydraulic retention time of 8 h.

2.2. Inoculum sludge and influent medium

The inoculated sludge for the reactors was obtained from secondary sedimentation tank in Beicang Wastewater Treatment Plant in Tianjin, China. The initial biomass concentration in all reactors was 3.7 g/L. Starch and protein were introduced as model polymers to prepare the influent medium. The influent medium including 600 mg/L chemical oxygen demand (COD), 60 mg/L ammonia nitrogen (NH₄⁺-N), 10 mg/L total phosphorous (TP), 20 mg/L Ca²⁺, 12 mg/L Mg²⁺, and 1 mL/L trace element solution. The composition details of the influent media were described in Supplementary Material (Table S1). The corresponding organic loads was 1.8 kg COD/(m³·d).

2.3. PHB/glycogen extraction and determination

20 mg dried sludge was used to extracted PHB and glycogen. PHB extraction method was as follows: 50 μ L benzoic acid-propanol solution, 1.5 mL propanol: HCl (4:1) solution and 1.5 mL 1,2 dichloroethane were mixed with the dried sludge samples. Then, the mixture was heated at 100 °C for 3 h. After cooling down, the sludge suspension was added into 2 mL ultrapure water, followed by 30-s vortex and 5-min centrifugation (3000 rpm) to obtain the supernatant. Gas Chromatograph (GC, Shimadzu, 2010-Plus, Japan) equipped with Stabilwax-DA column was used to determine PHB content. Glycogen extraction method: the dried sludge was digested at 120 °C with 0.6 mol/L HCl. Phenol-sulfuric acid method was used to measure glycogen content.

2.4. Sludge electrochemical property analysis

Cyclic voltammetry (CV) curve and electrochemical impedance spectroscopy (EIS) were conducted to investigate the electrochemical properties of sludge in four reactors using an electrochemical workstation (CHI-660E, China). The scanning rate of CV curve was 0.005 V/s, and the frequency range of EIS was 102~105. Conductive glass (1 \times 1 cm²) served as the working electrode, and a platinum sheet (1 \times 1 cm²) functioned as the counter electrode. An Ag/AgCl electrode was used as the reference electrode. The measured potential was modified based on the reversible hydrogen electrode (RHE) using the following Eq. (1) (Wang et al., 2022):

$$E_{\text{RHE}} = E_{\text{vs. Ag/AgCl}} + 0.059 * \text{pH} + 0.197V \quad (1)$$

2.5. Microbial community and assembly analysis

The microbial community in polymer-fed AGS system was analyzed by high-throughput sequencing technology (Si et al., 2025). The sludge samples for microbial community were collected on day 1 (seed sludge, denoted as S0), day 80 (R_C: C-1, R_E: E-1, R_{Fe}: Fe-1, R_{IE}: IE-1), day 120 (R_C: C-2, R_E: E-2, R_{Fe}: Fe-2, R_{IE}: IE-2), day 160 (R_C: C-3, R_E: E-3, R_{Fe}: Fe-3, R_{IE}: IE-3) and day 200 (R_C: C-4, R_E: E-4, R_{Fe}: Fe-4, R_{IE}: IE-4). The genomic DNA was extracted using E.Z.N.A. soil DNA kit (Omega Biotech, Norcross, GA, USA) according to manufacturer's protocols. The DNA purity and integrality were determined by NanoDrop2000 and agarose gel electrophoresis (AGE), respectively. The 16S rRNA gene between V3 and V4 regions was amplified by polymerase chain reaction (PCR) Amplifier (GeneAmp® 9700, ABI, USA) using primers of 338F (5'-ACTC CTACGGGAGGCAGCAG-3') and 806R (5'-GGACTTACHVGGGTWTCT AAT-3'). PCR production was sequenced via Illumina MiSeq platform (Majorbio Bio-Pharm Technology Co., Ltd., China). Principal Coordinate Analysis (PCoA) was conducted based on analysis of similarities (ANOSIM) and Bray-Curtis distance. Microbial assembly mechanism (deterministic and stochastic processes) was analyzed using Sloan

neutral community model (NCM) at OTU level.

2.6. Other analytical methods

Mixed liquid volatile suspended solid (MLVSS), sludge volume index at 5 min (SVI_5), COD, NH_4^+ -N and TP were measured in accordance with the standard methods (APHA, 2005). Mean particle size was determined by laser particle size analysis system (Malvern Mastersizer, 2000; England) and nano measurer 1.2. Scanning electron microscope (SEM, Nova Nano SEM450, USA) was used to examine sludge microstructure and morphology (Yang et al., 2023). Starch and protein were measured through starch-iodine method (San Pedro et al., 1994) and Lowry method (Bradford, 1976), respectively. Protease activity was measured according to a modified method (Zhu et al., 2021), and α -amylase activity was determined using 3,5-dinitrosalicylic acid (DNS) assay, the details were described in the supplementary material (Text S1). Cytochrome C (Cyt-C) was detected using ELISA kit (Shanghai Lanpai

Biotechnology Co., Ltd). Three-dimensional excitation-emission matrix (3D-EEM, Shimadzu CARY Eclipse, Japan) was performed to detect humic acid, with excited spectrum of 220~450 nm and emitted spectrum of 250~550 nm (Yu et al., 2023). The valence distribution of iron was detected by X-ray photoelectron spectroscope (XPS, Thermo ESCALAB 250Xi, USA). Statistical Package for the Social Sciences (SPSS) software was used to conduct the significance analyses by ANOVA test.

3. Result and discussions

3.1. Granule property analysis and stability evaluation

The variations in sludge properties, including granule morphology, biomass concentration and sludge settleability, were monitored during a 200-day operational period. Based on the observed changes, the operation was divided into three stages: Stage I (granulation period, 0–90 days), Stage II (stable period, 91–130 days) and stage III (deterioration

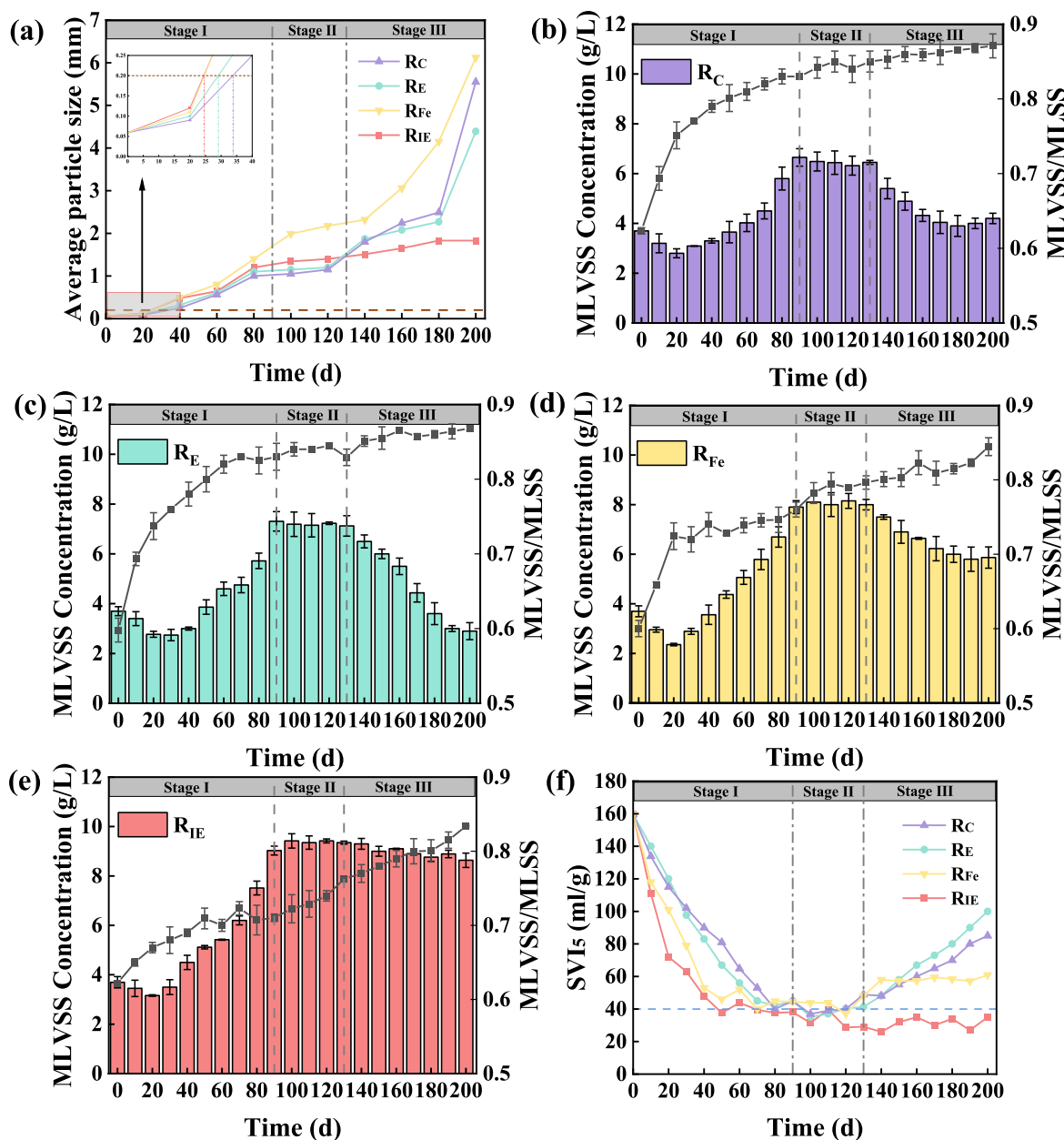


Fig. 1. Evolution of sludge properties during 200-day operation: (a) average particle size; (b ~ e) MLVSS concentration in R_C (b), R_E (c), R_{Fe} (d) and R_{IE} (e); (f) SVI_5 values.

period, 131–200 days). Fig. 1a illustrates the changes in average particle size across the control reactor (R_C), the electric field alone reactor (R_E), the iron ion alone reactor (R_{Fe}) and the iron electrolysis reactor (R_{IE}). It is clear that the mean granule size gradually increased and reached 1–2 mm during Stage II (91–130 days). Notably, the average particle size in R_{Fe} and R_{IE} reached 0.2 mm on day 25, which was shorter than that in R_C (34 days) and R_E (29 days). This result suggested that the presence of iron ions accelerated the formation of granules. Iron is known for its coagulation properties, which facilitated granulation process. However, with the extension of operational time (Stage III, 131–200 days), the granule size in R_C , R_E and R_{Fe} increased excessively, reaching 4.4–6.1 mm. On the contrary, the granules in R_{IE} maintained a consistent size of approximately 1.8 mm until the end of reactor operation (Fig. 1a). Microscope and SEM characterization revealed the granules developed in R_C , R_E and R_{Fe} were fluffy. These granules displayed excessive filamentous growth extending from their surface, resulting in large and loose structures with finger-like projections (Fig. 2a~l). Unlike the control reactors, the granules obtained from R_{IE} maintained smooth edges, fewer filaments and compact structures (Fig. 2m~p).

Biomass retention and sludge settleability were further evaluated by monitoring MLVSS and SVI₅ values. As shown in Fig. 1b~e, the MLVSS concentration initially increased and then stabilized at 6.7 ± 0.4 g/L (R_C), 7.3 ± 0.4 g/L (R_E), 7.9 ± 0.3 g/L (R_{Fe}) and 9.0 ± 0.2 g/L (R_{IE}) on day 90 with a ratio of food to microorganisms of 0.2–0.27 gCOD/gVSS-d. However, after day 130, biomass loss was observed in R_C , R_E

and R_{Fe} except for R_{IE} , as indicated by the decrease in biomass concentration with reductions of 34.9 % (R_C), 59.4 % (R_E) and 26.8 % (R_{Fe}). Meanwhile, the SVI₅ values increased rapidly from 41–49 mL/g (day 130) to 61–100 mL/g (day 200) in R_C , R_E and R_{Fe} . The poor settling performance should be responsible for the biomass loss in R_C , R_E and R_{Fe} . Notably, R_{IE} exhibited stable SVI₅ values of 29–35 mL/g, much lower than 61–100 mL/g determined in R_C , R_E and R_{Fe} . The excellent sludge settleability under iron electrolysis improved the biomass retention, avoiding biomass loss in polymer-fed AGS system.

Taken together, the filamentous overgrowth and granule deterioration were observed in R_C . This result is consistent with previous studies. Studies showed feeding with polymer typically drives filamentous overgrowth in AGS systems given the slow hydrolysis and limited PHB synthesis (de et al., 2010; Chen et al., 2024; Geng et al., 2025). For example, Geng et al. (2025) reported that feeding with polymers stimulated filamentous overgrowth with the extension of operational time, while the granules feeding with simple substrate (acetate) remained smooth and compact structure during 235-day operation time. Notably, deterioration of sludge properties was also observed in both R_{Fe} and R_E . This indicated the separate application of electric field or iron ions did not prevent the filamentous overgrowth in polymer-fed AGS system. Interestingly, smooth and stable granules were obtained in R_{IE} during the whole operation, implying that iron electrolysis effectively inhibited filamentous overgrowth and prevented granule deterioration. In this context, it can be reasonably inferred that the electric fields and iron

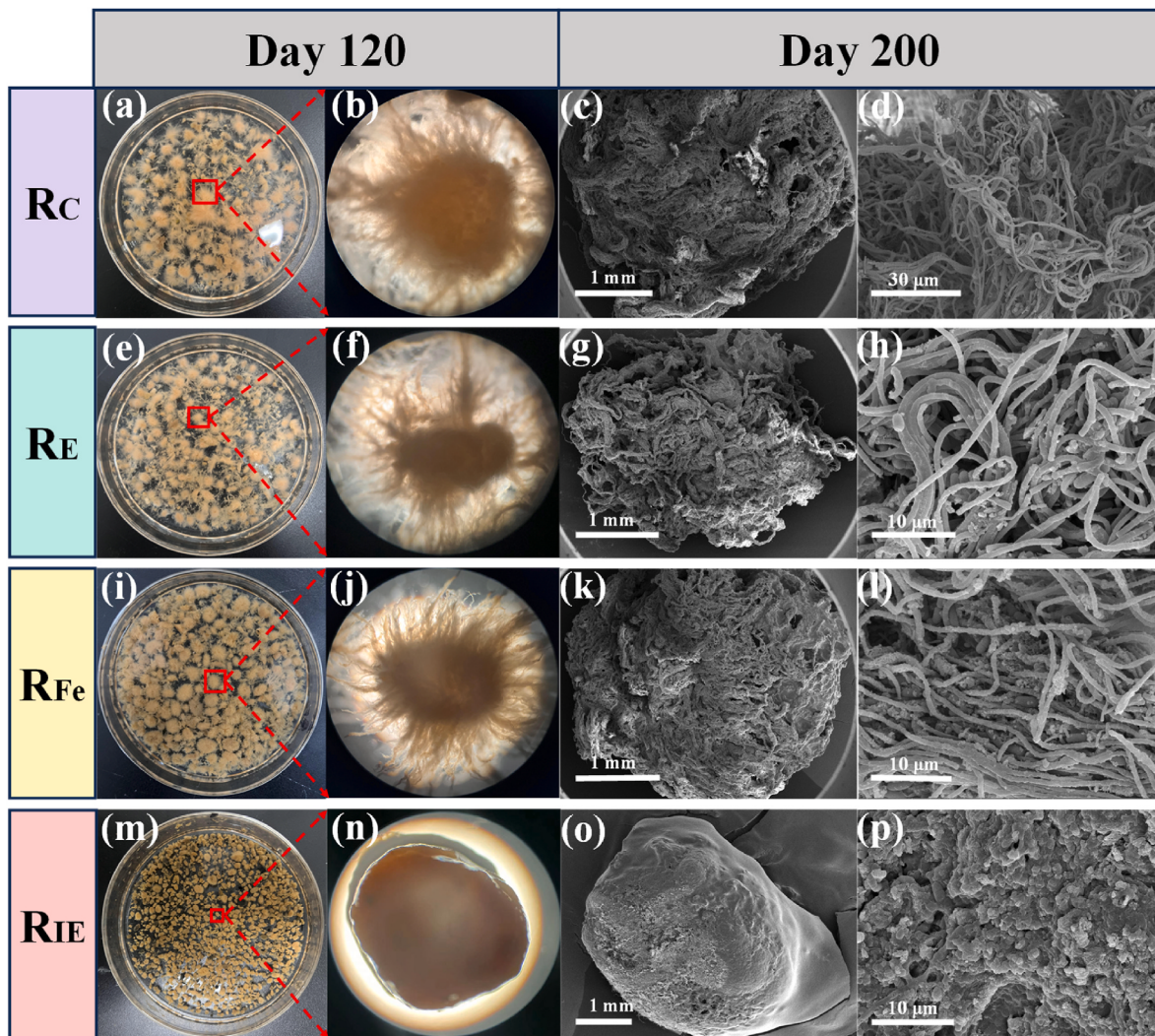


Fig. 2. AGS morphology variation in R_C , R_E , R_{Fe} and R_{IE} on day 120 and 200 (R_C : a-d, R_E : e-h, R_{Fe} : i-l, R_{IE} : m-p).

ions may have a synergistic effect on inhibiting filamentous overgrowth, solving the problem of granule instability induced by influent polymers.

3.2. PHB synthesis

Fig. 3a illustrates the overall substrate removal efficiency. Clearly visible is that the COD removal efficiencies in the R_C , R_E and R_{Fe} gradually declined with the extension of operational time during stage III, confirming the deterioration and instability of granule performance. The decrease in COD removal efficiency in R_C , R_E and R_{Fe} should be associated with the fluffy structure of the granules, which deteriorated sludge settleability and resulted in biomass washout, thus decreasing and destabilizing COD removal performance. Unlike the decrease in COD removal in the control reactors, the COD removal efficiency in R_{IE} consistently maintained at a high level of $94.3 \pm 0.6\%$, indicating efficient and stable performance in COD removal under iron electrolysis conditions. This was attributed to the compact and smooth granules,

which exhibited superior settling performance and ensured high biomass retention in R_{IE} , contributing to the efficient COD removal efficiency.

Furthermore, a batch test based on a typical operation cycle was conducted. As shown in **Fig. 3b~c**, the concentrations of starch and protein in the R_{IE} were $3.3 \pm 0.4 \text{ mg/L}$ and $4.3 \pm 0.6 \text{ mg/L}$ at the end of anaerobic period, respectively, which were lower than those in R_C , R_E and R_{Fe} . This result implied that R_{IE} achieved more efficient anaerobic polymer removal. **Fig. 3d** shows the contents of PHB and glycogen in the four reactors. It was noticed that R_{IE} synthesized more PHB compared to R_C , R_E and R_{Fe} . The accumulated PHB (ΔPHB) in R_{IE} reached the highest value of $20.6 \pm 1.6 \text{ mg/g VSS}$, higher than those in R_C ($11.6 \pm 2.0 \text{ mg/g VSS}$), R_E ($13.6 \pm 0.1 \text{ mg/g VSS}$) and R_{Fe} ($12.3 \pm 1.6 \text{ mg/g VSS}$). This finding suggested that the coexistence of the electric field and iron ions synergistically enhanced PHB storage in polymer-fed AGS system, facilitating the formation of smooth and stable granules in R_{IE} .

Further analysis showed that the α -amylase and protease in R_{IE} were

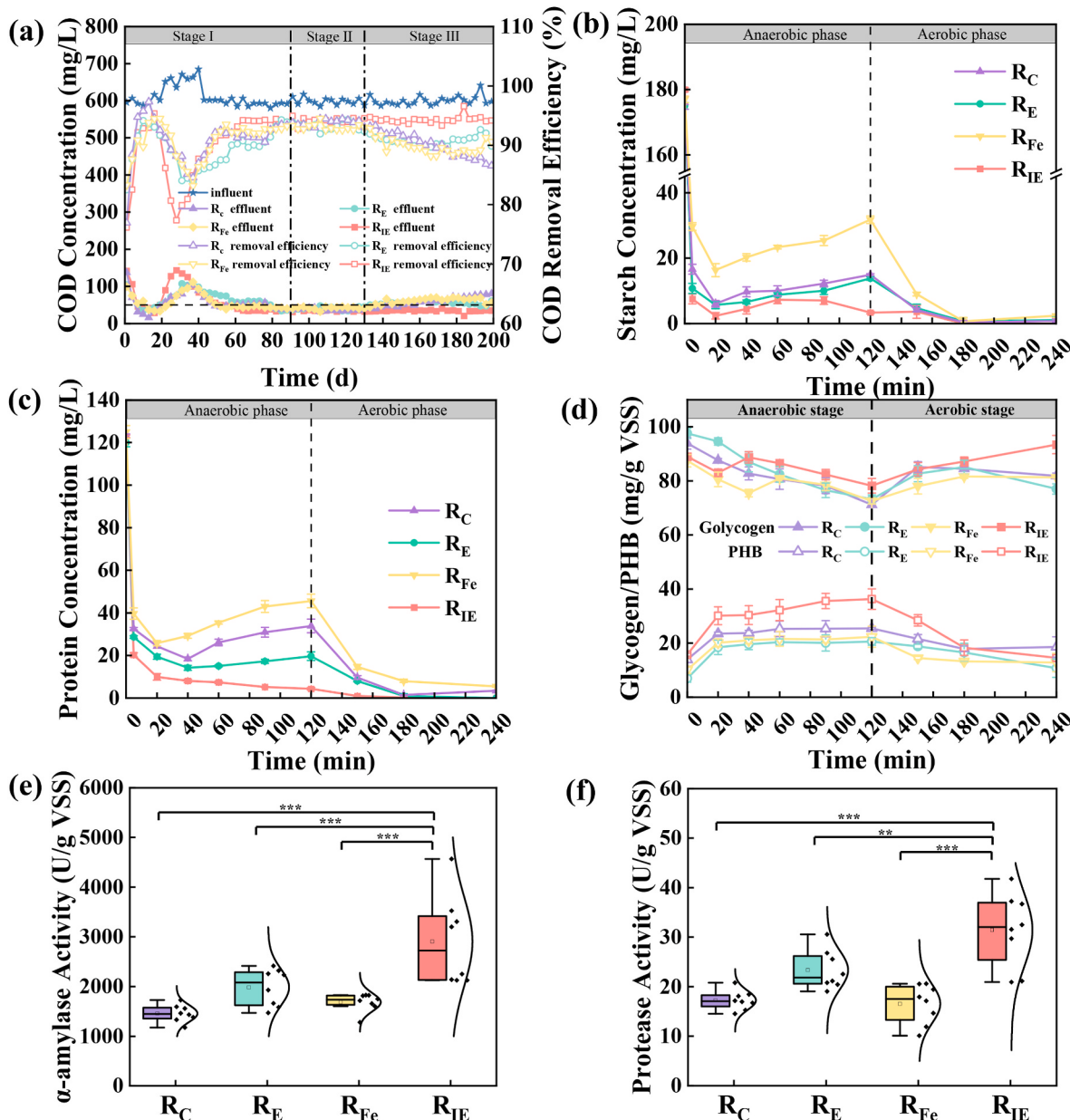


Fig. 3. Profiles of COD removal during 200-day operation (a); starch and protein concentration profiles during 4-h batch test (b ~ c); glycogen and PHB contents variations during 4-h batch test (d); protease and α -amylase activities (e, f) (*: $p < 0.05$, **: $p < 0.01$, *** $p < 0.001$).

the most active compared to those in R_C , R_E and R_{Fe} . Specifically, the average activities of α -amylase and protease in R_{IE} were 2905 U/gVSS and 31.4 U/gVSS, respectively, significantly higher than those in R_C , R_E and R_{Fe} (α -amylase: 1457–1984 U/gVSS; protease: 16.5–23.4 U/gVSS) ($p < 0.01$) (Fig. 3e and f). The high enzyme activities in R_{IE} suggested that iron and electricity enhanced the polymer hydrolysis process, improving the production of small molecular compounds and thereby increasing available substrates for synthesizing PHB. This well explained the efficient influent polymers conversion into PHB contents. As a result, most influent polymers were utilized during anaerobic period in R_{IE} , decreasing the substrates leakage to aerobic phase and creating substrate-deprived environment in the subsequent aerobic period. In this case, microbes have to relied on the stored PHB for survival. Previous studies documented that bacteria dependent on intercellular substrate like PHB exhibited much slower growth rates ($<2\text{ d}^{-1}$) compared to those utilizing exogenous substrates directly ($<2\text{ h}^{-1}$) (Elahinik et al., 2023). Haaksman et al. (2020) demonstrated that excess substrate leakage into the aerobic period stimulated the overgrowth of rapid-growing bacteria, promoting filamentous structure development. Overall, the application of iron electrolysis enhanced the uptake of influent polymers and PHB storage, thereby inhibiting excessive bacterial proliferation and facilitating the maintenance of granule structural stability.

3.3. Electron transfer capacity analysis

The sludge electrochemical properties were assessed using an electrochemical workstation to evaluate extracellular electron transfer capacities. Fig. 4a presents the CV curves, which were employed to identify the charge capacity within the AGS system (Rahman et al., 2023). Notably, distinct performances were observed across the four reactors. In the R_{IE} , the specific capacitance reached a maximum value of $4.1 \pm 0.3\text{ mF/g}$, higher than that of the R_C ($2.5 \pm 0.3\text{ mF/g}$), R_E ($2.3 \pm 0.2\text{ mF/g}$) and R_{Fe} ($3.6 \pm 0.3\text{ mF/g}$). This suggested a greater number of electron-storage sites involved in the electron exchange during the redox reaction process. Additionally, the CV curves indicated that both oxidation and reduction peaks in R_{IE} were more pronounced than those in the other reactors, reflecting higher current density and a more active redox process in R_{IE} (Xu et al., 2024). Both enhanced capacitance and intensified redox performance suggested superior electron storage capacity of the sludge in R_{IE} .

The extracellular electron transfer efficiency was further elucidated through electrochemical impedance spectroscopy (EIS) analysis. Fig. 4b displays the Nyquist plots with equivalent circuit fitting for the sludge samples from the four reactors. In the high-frequency range, the radius of the circular arc in R_{IE} was considerably smaller than that in R_C , R_E and R_{Fe} . The equivalent circuit fitting results indicated that the charge

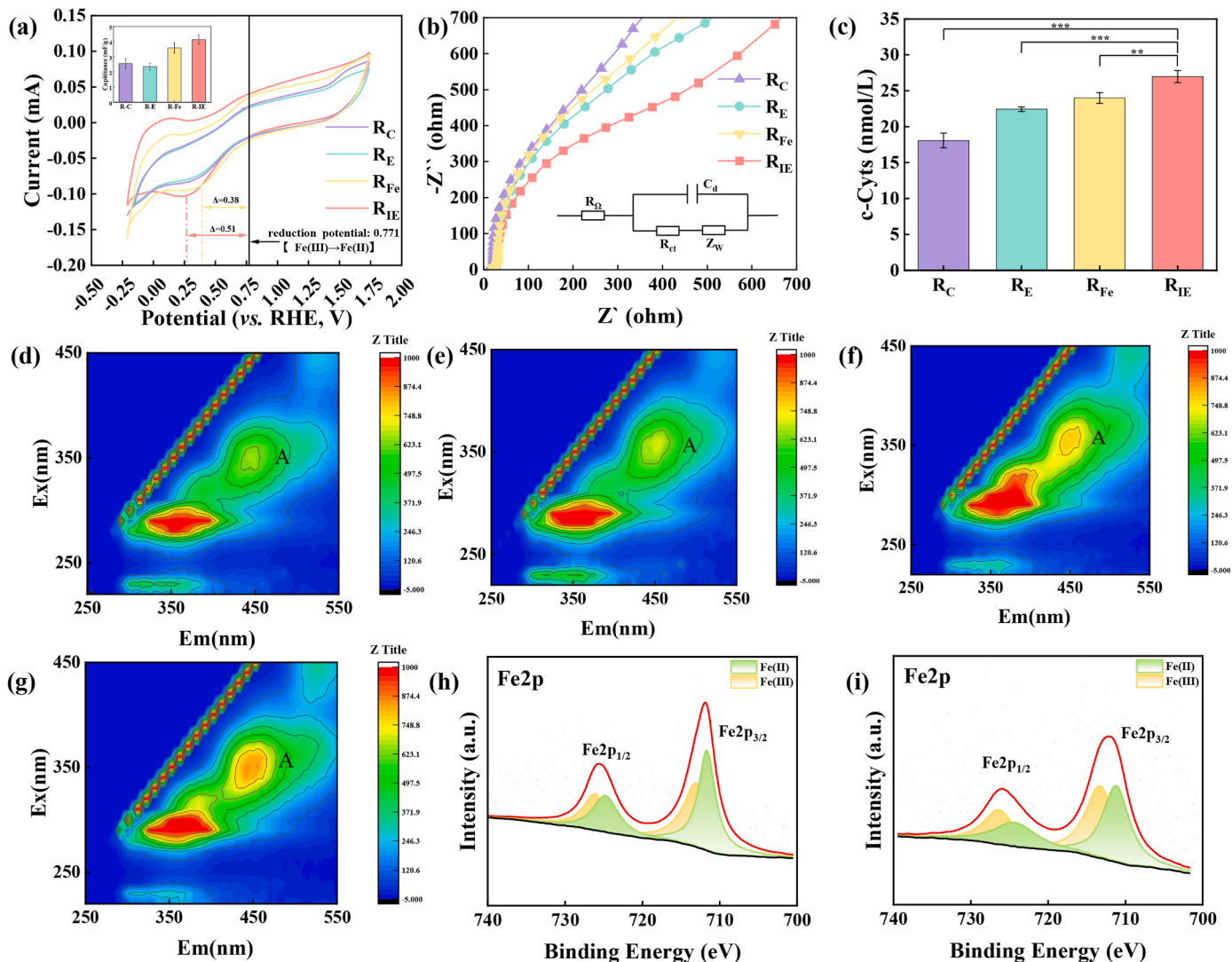


Fig. 4. Electrochemical properties of the sludge: (a) CV curves; (b) EIS fitted by equivalent circuit; (c) Cyt-C concentrations; (d ~ g) 3D-EEM spectra of HA (Peak A) in R_C (d), R_E (e), R_{Fe} (f) and R_{IE} (g); (h ~ i) XPS high-resolution spectra of Fe 2p in R_{IE} (h) and R_{Fe} (i). (*: $p < 0.05$, **: $p < 0.01$, ***: $p < 0.001$).

transfer resistance (R_{CT}) in R_{IE} was 680Ω , which was 40.1 %, 27.0 % and 38.5 % lower than the resistances of 1136Ω in R_C , 931Ω in R_E and 1105Ω in R_{Fe} , respectively. The reduced charge transfer resistance in R_{IE} reflected rapid electron transfer efficiency under iron electrolysis conditions. Collectively, both superior electron storage capacity and rapid electron transfer efficiency demonstrated that the AGS formed under iron electrolysis exhibited stronger electron transfer capacity compared to the control reactor, facilitating the efficient polymer utilization and PHB synthesis in R_{IE} .

It is known that microorganism exchanges electrons through secreting electroactive substances, such as cytochrome C (Cyt-C) (Guo et al., 2024; Tulsiyan et al., 2023). As a “bridge” connecting various microbes, the content of electroactive substance significantly influences microbial electron transfer performance (Li et al., 2022; Siddharth et al., 2021). As shown in Fig. 4c, the Cyt-C content in R_{IE} was 27.0 ± 0.9 nmol/L, which was higher than the levels found in R_{Fe} , R_E and R_C ($p < 0.01$). Besides that, 3D-EEM results showed that high humic acids (HA) were observed in R_{IE} compared to the control reactor. As shown in Fig. 4d~g, the peak A (Ex/Em of $330\text{--}379/430\text{--}465$ nm) exhibited the strongest fluorescence in R_{IE} , manifesting that iron electrolysis enhanced the HA content in polymer-fed AGS system. Similar to Cyt-C, HA has been widely recognized for its role in electron transfer process during organic degradation, acting as electron shuttles (Zhang et al., 2022a). These results implied that iron electrolysis stimulated the production of both Cyt-C and HA, well supported the efficient electron transfer performance in R_{IE} .

Furthermore, the valence distribution of iron during iron redox cycle was determined through XPS spectra analysis. As illustrated in Fig. 4h~i, the Fe $2p_{3/2}$ and Fe $2p_{1/2}$ spectra appeared at 712.2 and 726.0 eV, respectively, and were divided into Fe(II) and Fe(III) peaks. The binding energies for Fe(II) and Fe(III) were 711.7 and 713.1 eV in Fe $2p_{3/2}$, and 724.8 and 726.2 eV in Fe $2p_{1/2}$ (Feng et al., 2024). Quantitative analysis revealed that the content of Fe(II) accounted for 63.4 % of the total iron in R_{IE} , higher than the 45.1 % observed in R_{Fe} . This suggested enhanced reduction of Fe(III) to Fe(II) and a rapid iron redox cycle under iron electrolysis conditions. The increased reduction of Fe

(III) was further supported by greater reductive capability observed in the CV curves. The reduction potential (vs. RHE) for the Fe(III) to Fe(II) is $+0.771$ V, with reduction peaks in R_{IE} and R_{Fe} located at 0.261 V and 0.391 V, respectively (Fig. 4a). The larger potential difference in R_{IE} ($\Delta = 0.51$ V) compared to R_{Fe} promoted the reduction of Fe(III) to Fe(II) (Sun et al., 2024). These results implied that R_{IE} exhibited a rapid iron cycle. The enhanced iron cycle driven by electric field mainly include two processes: (i) iron (Fe) lost electrons to form Fe^{2+} , which were highly unstable and readily lost electrons to form Fe^{3+} very rapidly at the anode; and then these Fe^{3+} migrated to the cathode region, which was reduced to Fe^{2+} through accepting electrons from cathode, establishing iron cycle between anode and cathode (Pereira et al., 2023); (ii) functional microbes reduced the Fe^{3+} released from anode to Fe^{2+} , and these Fe^{2+} was oxidized by oxidizing bacteria, achieving iron cycle. It has been documented that the iron redox cycle can function as a bioelectrical capacitor or reservoir (Xu et al., 2024). The enhanced Fe (II)/Fe(III) redox cycle in R_{IE} provided evidences for the enhancement of electron transfer under iron electrolysis.

3.4. Microbial community structure

Microbial composition analysis based on phylum level showed that *Proteobacteria* and *Chloroflexi* were the most abundant phyla in R_C , constituting over 60 % of the total sequences (Fig. 5a), indicating the overgrowth of *Proteobacteria* and *Chloroflexi* in polymer-fed AGS system. Likewise, R_E and R_{Fe} exhibited similar populations to R_C , in which *Proteobacteria* and *Chloroflexi* were the top two phyla (Fig. 5a). This result demonstrated that the growth advantages of *Proteobacteria* and *Chloroflexi* were unaffected by the application of separate iron and electricity. By contrast, the microbial compositions in R_{IE} exhibited more even distribution, which was much different from that of R_C . PCoA analysis indicated that the distance between R_{IE} and R_C was the longest (Fig. 5b), reconfirming the different populations in R_{IE} compared to R_C . Specifically, the relative abundances of *Proteobacteria* and *Chloroflexi* were 14.0–16.7 % and 24.8–25.6 %, respectively, which were much lower than that in R_C , implying that iron electrolysis inhibited the

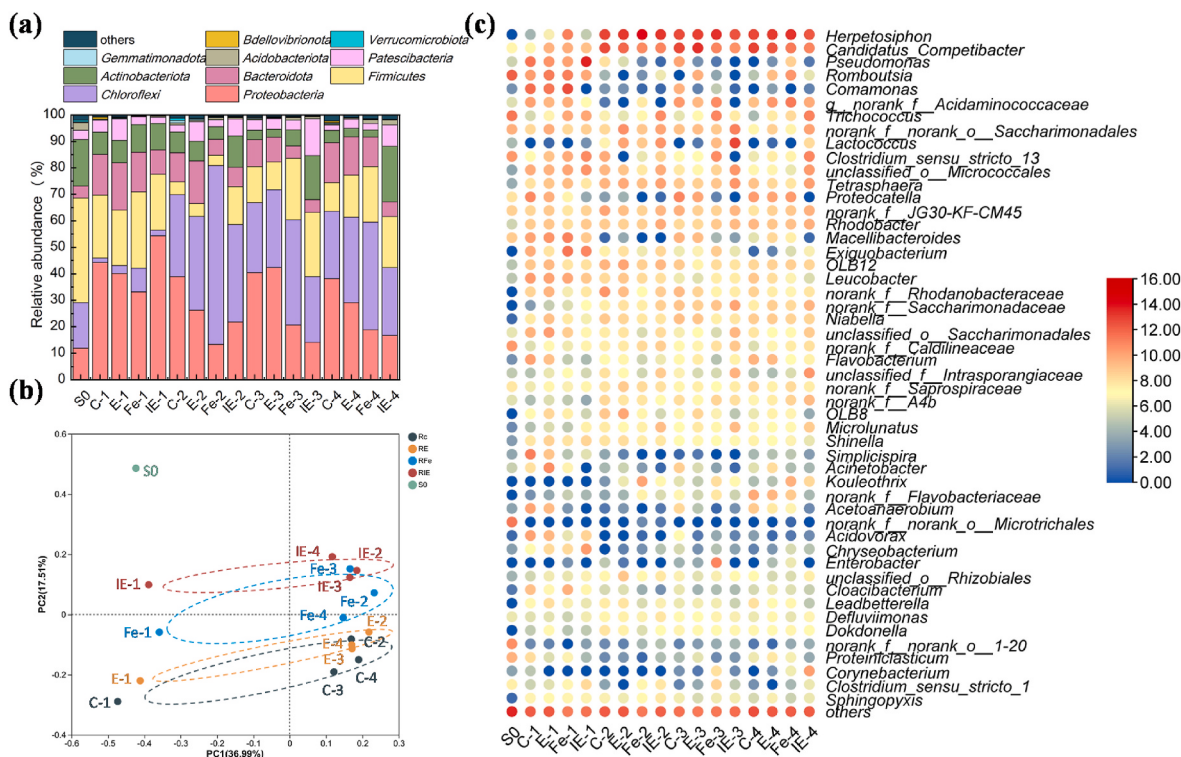


Fig. 5. Microbial community analysis: (a) microbial composition at phylum-level; (b) PCoA analysis based on OTU; (c) heat map at genus-level.

growth of phyla *Proteobacteria* and *Chloroflexi*. Further analysis showed that the genus *Herpetosiphon* was the main contributor to the abundance of phylum *Chloroflexi* (Fig. 5c), which has been identified as filamentous bacteria (Deng et al., 2021; Livingstone Paul et al., 2018). The higher abundance of *Herpetosiphon* in R_C (21.5–24.5 %), R_E (26.6–30.7 %) and R_{Fe} (33.8–60.2 %) confirmed filamentous overgrowth, suggesting that separate iron and electricity cannot prevent filamentous overgrowth in polymer-fed AGS system, which is consistent with the serious finger-type structure observed on granule surface (Fig. 2). Unlike the selective growth of filamentous bacteria (*Herpetosiphon*) in R_C, R_E and R_{Fe}, the relative abundance of *Herpetosiphon* in R_{IE} exhibited a lower value (7.7–18.6 %), demonstrating the inhibition of iron electrolysis on filamentous proliferation, facilitating granule dense structure and stability.

Moreover, iron electrolysis enriched genera norank_o_ *Saccharimonadales* (7.5–13.1 %), *Clostridium sensu stricto_13* (6~6.7 %), *Tetrasphaera* (4.0–4.8 %), *Trichococcus* (5.9–7.1 %) and *Lactococcus* (2.1–4.8 %), whose abundances were much higher than those in R_C, R_E and R_{Fe} with approximately 2.5–11.1 folds (Fig. 5c). Among above-mentioned genera, norank_o_ *Saccharimonadales*, *Lactococcus* and *Tetrasphaera* have been identified as hydrolytic and fermentative bacteria capable of degrading sugars into galactose, arabinose and lactic acid (Xi et al., 2023; Zhang et al., 2022b). Also, *Lactococcus* and *Tetrasphaera* have been considered as well-known protein degraders, producing proteolytic enzymes capable of breaking down protein molecules into peptides and amino acids (Marques et al., 2017; Close et al., 2021). The enhancement

of norank_o_ *Saccharimonadales*, *Tetrasphaera* and *Lactococcus* in R_{IE} indicated that iron electrolysis improved the growth of hydrolytic/fermentative bacteria in polymer-fed AGS system, which favored the production of smaller molecular weight compounds and thus for efficient influent polymer conversion into PHB. Additionally, more abundant electroactive microbes like *Clostridium sensu stricto_13* and *Trichococcus* were found in R_{IE} compared to R_C (Fig. 5c). Previous studies have reported that *Clostridium sensu stricto_13* and *Trichococcus* can transfer electrons to syntrophic microorganisms via oxidizing organics (Saheb-Alam et al., 2019; Nevin et al., 2011). Besides that, *Clostridium sensu stricto_13* and *Trichococcus* possessed iron-reducing function (Wang et al., 2024; Ma et al., 2021), potentially driving and contributing to iron redox cycle process. As such, the abundant electroactive/iron reduction bacteria in R_{IE} well explained the enhanced iron redox cycle and electrochemical properties.

3.5. Microbial assembly mechanism (stochasticity vs. determinacy)

Neutral Community Model (NCM) was conducted to analyze the assembly process (stochastic and deterministic pattern) that governed microbial community evolution in R_C, R_E, R_{Fe} and R_{IE}. In Fig. 6, it is clear that the goodness-of-fit (R^2) values in R_E (0.444), R_{Fe} (0.383) and R_{IE} (0.548) exhibited a higher level than R_C (0.354), implying a diminished effect of deterministic manner on population assembly (Liu et al., 2024). In other words, the application of separated iron/electricity and iron

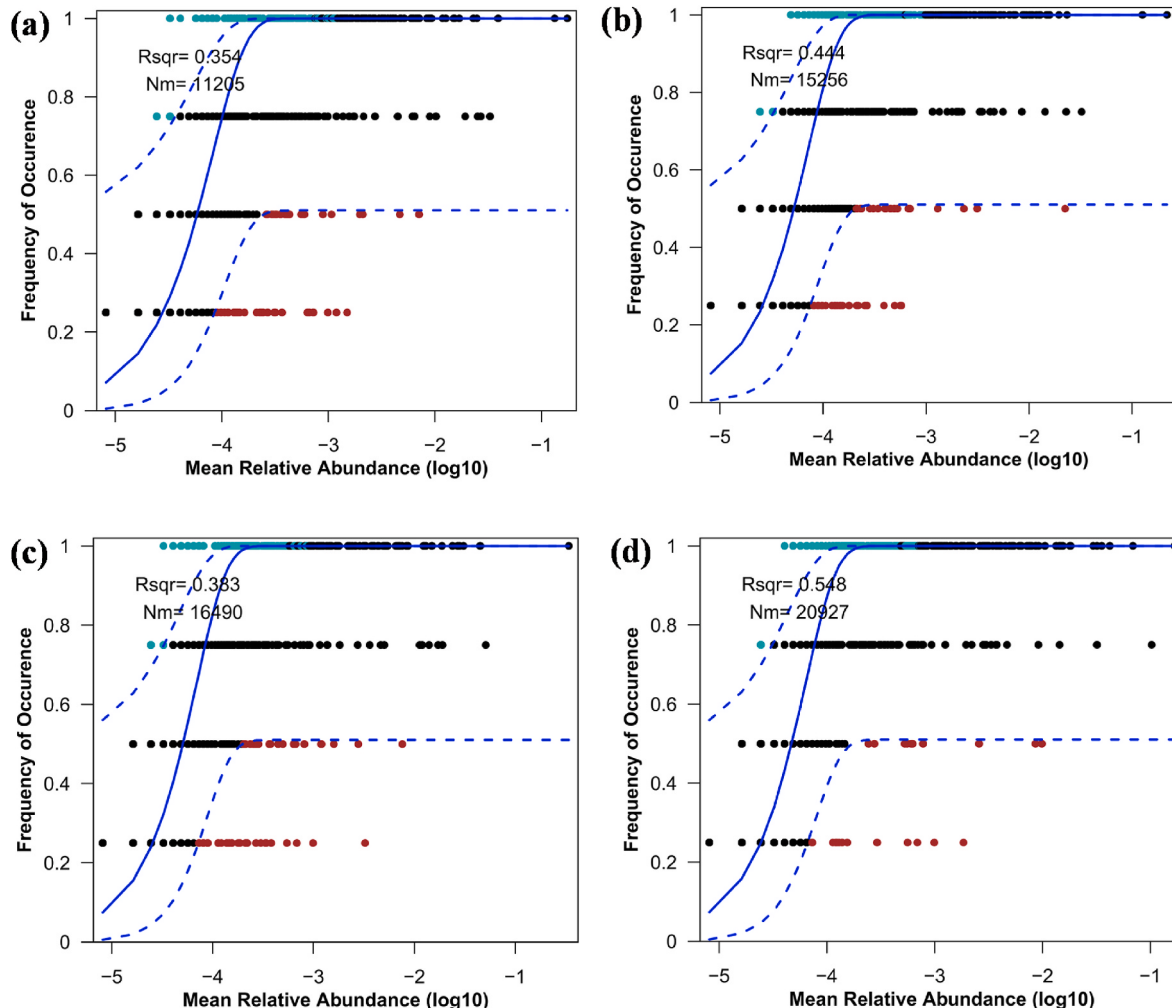


Fig. 6. Neutral Community Model (NCM) analysis based on OTU in R_C (a), R_E (b), R_{Fe} (c) and R_{IE} (d). Solid lines indicate the neutral-model prediction, and dashed lines represent 95 % confidence intervals. Note Nm = N*m, N represent OTU number, m indicates migration rate.

electrolysis enhanced the role of stochastic selection in shaping granule communities, especially iron electrolysis, as indicated by the largest R^2 value, highlighting the enhanced contributions of stochasticity in AGS system under iron electrolysis. In general, deterministic process was associated with higher selective pressure (Stegen et al., 2012; Okaiyeto et al., 2024). In AGS system, short settling time created an extreme environment for microbial growth. Slow settlers were washed out and the biomass with good settleability was retained, deterministically selecting microbial composition in AGS system. By contrast, iron electrolysis improved biomass aggregation and sludge settleability during granule formation phase (0–40 days), weakening the selective pressure and favoring biomass retention through non-selective attachment. Besides that, it has been proved that polymers were mainly hydrolyzed on granule surface and the produced substrates were subsequently consumed locally, increasing substrate gradient and inducing preferential growth of filamentous organisms due to the stronger competition of filaments than non-filaments under micro-gradient condition (de et al., 2010; Toja et al., 2022). This was also confirmed by the much high relative abundance of filamentous bacteria and excess growth of finger-type structures in R_c , R_E and R_{Fe} (Fig. 2). The selection of filamentous microbes appears to explain the deterministic assembly determined in AGS system. As for R_{IE} , iron electrolysis enhanced polymer hydrolysis and electron transfer in AGS system, increasing available substrate (compounds with smaller molecular weight) in polymer-fed AGS system. This favored various bacteria survival located inside granules instead of deterministic selection of filamentous bacteria, as indicated by the lowest relative abundance of filaments in R_{IE} (Fig. 2m~p). Based on the above-mentioned discussion, both enhanced biomass aggregation and nutrient availability under iron electrolysis weakened the importance of deterministic process and increased the contribution of stochasticity. Furthermore, compared with the deterministic selection of a certain bacteria, stochastic assembly could be beneficial for population diversity during microbial assembly. As shown in Table S2, the Shannon index values in R_{IE} displayed the highest level among four reactors. The high bio-diversity behaved various ecological niches and facilitated the stability of overall ecosystem (Shi et al., 2024). In this case, the enhanced stochastic assembly process appears to provide explanation for the stable state in R_{IE} during long-term operation.

4. Conclusion

This study represents an initial effort to investigate the feasibility of iron electrolysis strategy for inhibiting filamentous overgrowth in polymer-fed AGS system, providing a targeted strategy for enhancing the operation stability of AGS system during engineered application. The key findings include:

- (1) Iron electrolysis inhibited excessive filamentous structures growth on granule surface, effectively enhancing the operational stability of the polymer-fed AGS system.
- (2) Iron electrolysis enhanced hydrolytic enzyme activity and electron transfer capacity, favoring influent polymer conversion into PHB and thus inhibiting filamentous structure overgrowth.
- (3) Hydrolytic and electroactive bacteria were enriched in polymer-fed AGS system under iron electrolysis.

CRediT authorship contribution statement

Mingyue Geng: Writing – review & editing, Writing – original draft, Supervision, Formal analysis, Conceptualization. **Deyi Kong:** Writing – original draft, Investigation, Formal analysis. **Shanshan Gao:** Writing – review & editing. **Fangshu Qu:** Writing – review & editing, Supervision, Conceptualization. **Jiayu Tian:** Writing – review & editing, Supervision, Conceptualization.

Declaration of competing interest

The authors declare that they have no known competing financial interests or personal relationships that could have appeared to influence the work reported in this paper.

Acknowledgement

This work was supported by the National Natural Science Foundation of China (No. 52370035, 52400030), the Natural Science Foundation of Hebei Province, China (No. E2023202064) and China Postdoctoral Science Foundation (2024M750717).

Appendix A. Supplementary data

Supplementary data to this article can be found online at <https://doi.org/10.1016/j.jenvman.2025.126673>.

Data availability

Data will be made available on request.

References

- Amancio Frutuoso, F.K., da Silva, V.E.P.S.G., Silva, T.F.C.V., Vilar, V.J.P., Bezerra dos Santos, A., 2025. Solids retention time (SRT) control in the co-treatment of leachate with domestic sewage in aerobic granular sludge systems: impacts on system performance, operational stability, and bioresource production. *Bioresour. Technol.* 415, 131664.
- APHA, 2005. Standard Methods for the Examination of Water and Wastewater. American Public Health Association, Washington, DC, USA.
- Bradford, M.M., 1976. A rapid and sensitive method for the quantitation of microgram quantities of protein utilizing the principle of protein-dye binding. *Anal. Biochem.* 72, 248–254.
- Chen, X., Gong, Y., Li, Z., Guo, Y., Zhang, H., Hu, B., Yang, W., Cao, Y., Mu, R., 2024. Key function of *Kouleothrix* in stable formation of filamentous aerobic granular sludge at low superficial gas velocity with polymeric substrates. *Bioresour. Technol.* 397, 130466.
- Close, K., Marques, R., Carvalho, V.C.F., Freitas, E.B., Reis, M.A.M., Carvalho, G., Oehmen, A., 2021. The storage compounds associated with *Tetrasphaera PAO* metabolism and the relationship between diversity and P removal. *Water Res.* 204, 117621.
- de Kreuk, M.K., Kishida, N., Tsuneda, S., van Loosdrecht, M.C.M., 2010. Behavior of polymeric substrates in an aerobic granular sludge system. *Water Res.* 44, 5929–5938.
- Deng, M., Dai, Z., Song, K., Wang, Y., He, X., 2021. Integrating microbial protein production and harvest systems into pilot-scale recirculating aquaculture systems for sustainable resource recovery: linking nitrogen recovery to microbial communities. *Environ. Sci. Technol.* 55, 16735–16746.
- Elahinik, A., Li, L., Pabst, M., Abbas, B., Xevgenos, D., van Loosdrecht, M.C.M., Pronk, M., 2023. Aerobic granular sludge phosphate removal using glucose. *Water Res.* 247, 120776.
- Feng, L., Mu, H., Gao, Z., Hu, T., He, S., Liu, Y., You, S., Zhao, Q., Wei, L., 2024. Comprehensive insights into the impact of magnetic biochar on protein hydrolysis in sludge anaerobic digestion: protein structures, microbial activities and syntrophic metabolisms. *Water Res.* 260, 121963.
- Franca, R.D.G., Pinheiro, H.M., van Loosdrecht, M.C.M., Lourenço, N.D., 2018. Stability of aerobic granules during long-term bioreactor operation. *Biotechnol. Adv.* 36, 228–246.
- Geng, M., Li, T., Qu, F., Gao, S., Tian, J., 2025. Insights into the impact of feeding with polymers on aerobic granular sludge development and stability: performance and mechanisms. *Bioresour. Technol.* 426, 132368.
- Guo, Y., Shi, W., Zhang, B., Li, W., Lens, P.N.L., 2021. Effect of voltage intensity on the nutrient removal performance and microbial community in the iron electrolysis-integrated aerobic granular sludge system. *Environ. Pollut.* 274, 116604.
- Guo, Z., Qu, F., Wang, J., Geng, M., Gao, S., Tian, J., 2024. Enhancing electron transfer in anaerobic process by supercapacitor materials: polyaniline functioned activated carbon. *Bioresour. Technol.* 406, 131051.
- Guzmán-Pierro, V., Arriagada, C., Gallardo, J.J., Campos, V., Roeckel, M., 2023. Challenges of aerobic granular sludge utilization: fast start-up strategies and cationic pollutant removal. *Heliyon* 9, e13503.
- Haaksman, V.A., Mirghorayshi, M., van Loosdrecht, M.C.M., Pronk, M., 2020. Impact of aerobic availability of readily biodegradable COD on morphological stability of aerobic granular sludge. *Water Res.* 187, 116402.
- Han, X., Jin, Y., Yu, J., 2022. Rapid formation of aerobic granular sludge by bioaugmentation technology: a review. *Chem. Eng. J.* 437, 134971.
- He, J., Yao, J., Jiang, W., Aborisade, M.A., Liu, X., Zhang, Y., Deng, K., Chu, Z., 2024. Optimizing the formation of aerobic granular sludge and enhanced pollutant

- removal efficiency in a constant current variable voltage electric field. *J. Clean. Prod.* 438, 140721.
- Kong, Y., Liu, H., Chen, X., Su, K., Hu, Z., Kong, Z., Hao, T., 2022. Analysis of aerobic granulation trigger driving mechanism under different organic substrate diffusibility based on microfluidic system. *J. Water Proc. Eng.* 49, 103166.
- Li, N., Quan, X., Zhuo, M., Zhang, X., Quan, Y., Liang, P., 2022. Enhancing methanogenesis of anaerobic granular sludge by incorporating Fe/Fe oxides nanoparticles aided with biofilm disassembly agents and mediating redox activity of extracellular polymer substances. *Water Res.* 216, 118293.
- Li, Y., Guo, M., Kong, X., Jia, X., Zhao, X., 2024. Coupling micro-electric field into aerobic granular sludge system for sulfadiazine abatement: performance, mechanism, toxicity, and microbial characteristics. *Chem. Eng. J.* 483, 149258.
- Liang, H., Cui, Y., Yan, H., Li, Z., 2025. Recovery of disintegrated halophilic aerobic granular sludge through ferric ion addition: dual roles in filamentous fungal inhibition and microbial adhesion enhancement. *Water Res.* 283, 123844.
- Liú, S., Xia, S., Zhang, X., Cai, X., Yang, J., Hu, Y., Zhou, S., Wang, H., 2024. Microbial communities exhibit distinct diversities and assembly mechanisms in rainwater and tap-water storage systems. *Water Res.* 253, 121305.
- Livingstone Paul, G., Morphew Russell, M., Cookson Alan, R., Whitworth David, E., 2018. Genome analysis, metabolic potential, and predatory capabilities of *herpetosiphon lansteffanense* sp. nov. *Appl. Environ. Microbiol.* 84, 01040-01018.
- Lu, X., Yan, G., Fu, L., Cui, B., Wang, J., Zhou, D., 2023. A review of filamentous sludge bulking controls from conventional methods to emerging quorum quenching strategies. *Water Res.* 236, 119922.
- Ma, K., Wang, W., Liu, Y., Bao, L., Cui, Y., Kang, W., Wu, Q., Xin, X., 2021. Insight into the performance and microbial community profiles of magnetite-amended anaerobic digestion: varying promotion effects at increased loads. *Bioresour. Technol.* 329, 124928.
- Marques, R., Santos, J., Nguyen, H., Carvalho, G., Noronha, J.P., Nielsen, P.H., Reis, M.A. M., Oehmen, A., 2017. Metabolism and ecological niche of *Tetrasphaera* and *Ca. Accumulibacter* in enhanced biological phosphorus removal. *Water Res.* 122, 159–171.
- Nancharaiah, Y.V., Kiran Kumar Reddy, G., 2018. Aerobic granular sludge technology: mechanisms of granulation and biotechnological applications. *Bioresour. Technol.* 247, 1128–1143.
- Nevin Kelly, P., Hensley Sarah, A., Franks Ashley, E., Summers Zarath, M., Ou, J., Woodard Trevor, L., Snoeyenbos-West Oona, L., Lovley Derek, R., 2011. Electrosynthesis of organic compounds from carbon dioxide is catalyzed by a diversity of acetogenic microorganisms. *Appl. Environ. Microbiol.* 77, 2882–2886.
- Okaiyeto, S.A., Sutar, P.P., Chen, C., Ni, J.-B., Wang, J., Mujumdar, A.S., Zhang, J., Xu, M., Fang, X., Zhang, C., Xiao, H.-W., 2024. Antibiotic resistant bacteria in food systems: current status, resistance mechanisms, and mitigation strategies. *Agriculture Communications* 2, 100027.
- Pereira, J., Neves, P., Nemanic, V., Pereira, M.A., Sleutels, T., Hamelers, B., Heijne, A.t., 2023. Starvation combined with constant anode potential triggers intracellular electron storage in electro-active biofilms. *Water Res.* 242, 120278.
- Rahman, M.M., Shawon, M.R., Rahman, M.H., Alam, I., Faruk, M.O., Khan, M.M.R., Okoli, O., 2023. Synthesis of polyaniline-graphene oxide based ternary nanocomposite for supercapacitor application. *J. Energy Storage* 67, 107615.
- Saheb-Alam, S., Persson, F., Wilén, B.-M., Hermansson, M., Modin, O., 2019. Response to starvation and microbial community composition in microbial fuel cells enriched on different electron donors. *Microb. Biotechnol.* 12, 962–975.
- San Pedro, D.C., Mino, T., Matsuo, T., 1994. Evaluation of the rate of hydrolysis of slowly biodegradable COD (SBCOD) using starch as substrate under anaerobic, anoxic and aerobic conditions. *Water Sci. Technol.* 30, 191–199.
- Shi, X., Wang, L., Chen, A., Yu, W., Liu, Y., Huang, X., Long, X., Du, Y., Qu, D., 2024. Enhancing water quality and ecosystems of reclaimed water-replenished river: a case study of Dongsha River, Beijing, China. *Sci. Total Environ.* 926, 172024.
- Si, Q., Feng, X., Teng, Y., Shi, H., Kuang, J., Xiao, Z., Wang, W., Jiang, C., Guo, W., Ren, N., 2025. Constructing effective and low-toxic removal of combined contaminants by intimately coupled Z-scheme heterojunction photocatalysis and biodegradation system. *Appl. Catal. B Environ.* 365, 124909.
- Siddharth, T., Sridhar, P., Vinila, V., Tyagi, R.D., 2021. Environmental applications of microbial extracellular polymeric substance (EPS): a review. *J. Environ. Manag.* 287, 112307.
- Stegen, J.C., Lin, X., Konopka, A.E., Fredrickson, J.K., 2012. Stochastic and deterministic assembly processes in subsurface microbial communities. *ISME J.* 6, 1653–1664.
- Sun, X., Chen, H., Cui, T., Zhao, L., Wang, C., Zhu, X., Yang, T., Yin, Y., 2024. Enhanced medium-chain fatty acid production from sewage sludge by combined electro-fermentation and anaerobic fermentation. *Bioresour. Technol.* 404, 130917.
- Toja Ortega, S., Pronk, M., de Kreuk, M.K., 2021. Anaerobic hydrolysis of complex substrates in full-scale aerobic granular sludge: enzymatic activity determined in different sludge fractions. *Appl. Microbiol. Biotechnol.* 105, 6073–6086.
- Toja Ortega, S., van den Berg, L., Pronk, M., de Kreuk, M.K., 2022. Hydrolytic capacity of different sized granules in a full-scale aerobic granular sludge (AGS) reactor. *Water Res.* X 16, 100151.
- Tulsiyan, K.D., Mahalik, A., Dandekar, B.R., Mondal, J., Biswal, H.S., 2023. Enhancement of peroxidase activity in magnetic ionic liquids. *ACS Sustain. Chem. Eng.* 11, 8487–8494.
- Wang, L., Wu, Y., Fu, Y., Deng, L., Wang, Y., Ren, Y., Zhang, H., 2022. Low electric field assisted surface conductive membrane in AnMBR: strengthening effect and fouling behavior. *Chem. Eng. J.* 431, 133185.
- Wang, G., Song, J., Zhang, Z., Xiao, Q., He, S., Zeng, T., Liu, Y., Li, S., 2024. Enhanced indigenous consortia for the remediation of uranium-contaminated groundwater by bioaugmentation: reducing and phosphate-solubilizing consortia. *Sci. Total Environ.* 912, 168954.
- Winkler, M.K.H., Bassin, J.P., Kleerebezem, R., de Bruin, L.M.M., van den Brand, T.P.H., van Loosdrecht, M.C.M., 2011. Selective sludge removal in a segregated aerobic granular biomass system as a strategy to control PAO-GAO competition at high temperatures. *Water Res.* 45, 3291–3299.
- Xi, S., Dong, X., Lin, Q., Li, X., Ma, J., Zan, F., Biswal, B.K., Awasthi, M.K., Wang, Z., Chen, G., Guo, G., 2023. Enhancing anaerobic fermentation of waste activated sludge by investigating multiple electrochemical pretreatment conditions: performance, modeling and microbial dynamics. *Bioresour. Technol.* 368, 128364.
- Xu, H., Wang, M., Hei, S., Qi, X., Zhang, X., Liang, P., Fu, W., Pan, B., Huang, X., 2024. Neglected role of iron redox cycle in direct interspecies electron transfer in anaerobic methanogenesis: inspired from biogeochemical processes. *Water Res.* 262, 122125.
- Yang, H., Liu, Q., Shu, X., Yu, H., Rong, H., Qu, F., Liang, H., 2023. Simultaneous ammonium and water recovery from landfill leachate using an integrated two-stage membrane distillation. *Water Res.* 240, 120080.
- Yu, H., Huang, H., Zhong, L., Wu, S., Yang, H., Rong, H., Liang, H., Qu, F., Ma, J., 2023. Evaluation of front-face fluorescence for assessing Cyanobacteria fouling in ultrafiltration. *Environ. Sci. Technol.* 57, 17649–17658.
- Zhang, H., Quan, H., Zhou, S., Sun, L., Lu, H., 2022a. Enhanced performance and electron transfer of sulfur-mediated biological process under polyethylene terephthalate microplastics exposure. *Water Res.* 223, 119038.
- Zhang, M., Tan, Y., Fan, Y., Gao, J., Liu, Y., Lv, X., Ge, L., Wu, J., 2022b. Nitrite accumulation, denitrification kinetic and microbial evolution in the partial denitrification process: the combined effects of carbon source and nitrate concentration. *Bioresour. Technol.* 361, 127604.
- Zhu, W., Luan, H., Bu, Y., Li, J., Li, X., Zhang, Y., 2021. Changes in taste substances during fermentation of fish sauce and the correlation with protease activity. *Food Res. Int.* 144, 110349.